Impact of Substrate Imperfections on Epitaxial Layer Quality

Michael Wojtowicz, Randy Sandhu, Ben Heying, and Thomas Block
Northrop Grumman Space Technology
One Space Park, R6/2134, Redondo Beach, CA 90278
(310)814-1713 / mike.wojtowicz@trw.com

Ben Poust and Mark Goorsky
Department of Materials Science and Engineering
University of California, Los Angeles, CA 90095
(310)206-0267 / goorsky@seas.ucla.edu

ABSTRACT

We examined the role of substrate quality on the epitaxial layer structure and performance of pseudomorphic InGaAs/AlGaAs/GaAs and AlGaN/GaN/SiC high electron mobility transistors (HEMTs). High resolution x-ray diffraction, high resolution x-ray topography, and transmission electron microscopy proved essential. For the GaAs-based pseudomorphic HEMT (pHEMT), the epitaxial layer misfit dislocation density is always lower for a given channel composition and thickness when grown on substrates with lower threading dislocation densities. Furthermore, device electrical performance can be improved through increasing the channel thickness to a greater degree when grown on lower threading dislocation substrates. For the GaN-based HEMTs, the SiC substrates show scratches, micropipes, and various crystal distortions that impact the quality of the epitaxial material. High resolution x-ray topographs of processed HEMT materials enable evaluation of the impact of both micropipes and crystal distortion on the device performance.

INTRODUCTION

High quality, uniform substrates are critical to achieve the high quality, uniform epitaxial materials required for high performance HEMT MMICs. Understanding the interactions between substrate imperfections and subsequent epitaxial growth is critical for increasing the HEMT performance and yields. In addition, an understanding how substrate imperfections impact device performance is critical for developing the next generation of III-V HEMT materials, such as GaN/AlGaN. We will present the impact of substrate imperfections on device performance for InGaAs/(Al,Ga)As pHEMTs grown on GaAs substrates and AlGaN/GaN HEMTs grown on SiC substrates.

AlGaAs/InGaAs/GaAs pHEMT

High performance InGaAs/(Al,Ga)As pHEMTs are used in many applications ranging from wireless LANs, wireless cable broadcast transmitters and PCS microcell transponders for the commercial market [1] and smart munitions and satellite crosslinks for DoD applications. Power amplifiers operating above 100 GHz have been demonstrated [2]. However, there is a continuous effort to achieve more performance from these pHEMTs. Engineering the channel properties by increasing the channel indium composition and increasing the channel thickness provides increased performance. Understanding the interactions between substrate imperfections and subsequent epitaxial growth and pHEMT device performance is critical to increasing performance.

We report here the impact of GaAs substrate threading dislocation density on the material and electrical properties of $Al_{0.25}Ga_{0.75}As/In_{0.21}Ga_{0.79}As/GaAs$ pHEMTs. The maximum channel thickness and indium composition are influenced by the threading dislocation density in the GaAs substrate. The threading dislocations serve as nucleation sites for misfit dislocations that form at the strained pseudomorphic channel layer interface once the channel critical thickness is exceeded.

The HEMT structures used in this study were grown by molecular beam epitaxy (MBE). The baseline structure is illustrated in figure 1. Typical 300K channel carrier concentration of similar structures that have the ohmic cap layer (50 nm n^+ GaAs) removed are 3.5×10^{12} cm^{-2} with mobilities > 5,000 cm^2/V-s as measured by Hall effect. For this study, we varied the InGaAs channel thickness from 13 nm to 22 nm to evaluate the effect of the substrate threading dislocations on the strained channel layer relaxation. The epitaxial layer profile composition and thickness was determined by fitting double axis x-ray rocking curves. These pHEMT structures were grown on semi-insulating (SI) GaAs substrates with reported etch pit densities of <5,000 cm^{-2} and <50,000 cm^{-2}. We will refer to these wafers as low (LTDD) and high threading dislocation density (HTDD) substrates, respectively. The processed devices feature 2 μm source-drain spacing, 0.15 μm gate widths, source vias, and airbridge gates. The gates are oriented along the <110> direction.

The threading dislocation densities of the substrates were verified by counting the threads observed in curved crystal x-ray topography photographs [3]. The threading dislocations in the LTDD substrates were indeed <5000 cm^{-2} (nominally around 3,000 cm^{-2}). The density in the HTDD substrates was high enough that we could not distinguish individual dislocations.
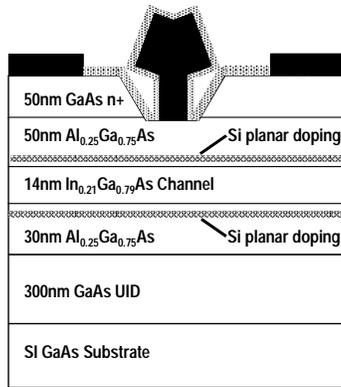
Figure 1. Baseline pHEMT material profile

Double axis measurements are typically used to assess the substrate quality. However, due to the large angular acceptance of the detector, double axis measurements can be relatively insensitive to the substrate quality. Double axis rocking curves from the LTDD and HTDD substrates have almost identical full-width at half-maximum values of 13 and 15 arcsec, respectively. High-resolution triple axis reciprocal space maps more clearly differentiate between the two types of substrates. Figure 2 shows the reciprocal space maps for both types of substrates. The axis Δq_{110} represents the degree of strain and the axis Δq_{004} represents the degree of mosaic tilt [4]. The reciprocal space map for the HTDD substrate includes diffuse scatter (broadening) symmetrically distributed around the peak. This scatter originates from the cellular structure of the substrate threading dislocations [3]. In the LTDD substrate, the tilt between adjacent cells is smaller since the density of dislocations is also smaller than the HTDD substrates. Thus, the difference in broadening exhibited in the reciprocal space maps is due the difference in the threading dislocation density.
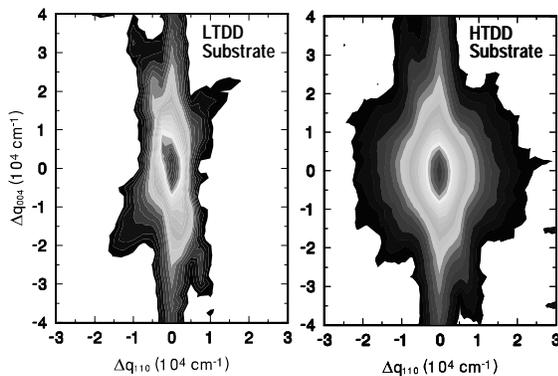

Figure 2. Reciprocal space maps of the (004) GaAs substrate reflection showing greater diffuse scatter in HTDD substrates.

Plan-view transmission electron microscopy (TEM) was used to determine the misfit dislocation densities in the device epitaxial layer for different channel thicknesses. Figure 3 shows the bright field TEM micrographs for a pHEMT device with a 15.5 nm and 15.0 nm channel thickness grown on a LTDD and HTDD substrates. The

misfit dislocation density along the <110> direction is approximately 0.3 μm^{-1} and 0.7 μm^{-1} for the LTDD and HTDD substrates, respectively. Figure 4 shows the TEM micrograph for a channel thickness of 22 nm and 21 nm grown on LTDD and HTDD substrates. The misfit dislocation densities along the <110> direction are approximately 1.0 μm^{-1} and 2.6 μm^{-1}, respectively. In addition, the thicker channel structures exhibit orthogonal arrays of misfit dislocations. The orthogonal dislocations nominally occur for channel thickness in excess of 20 nm [5, 6]. This clearly shows that the HTDD enhance the relaxation of the strained InGaAs channel layers and that the LTDD substrates result in greater epitaxial material layer quality.
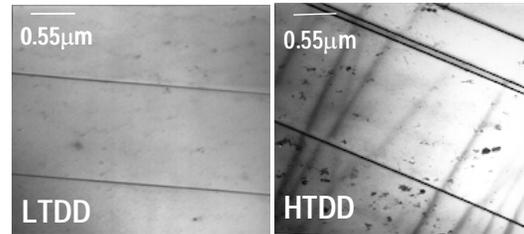

Figure 3. Plan-view TEM image of $In_{0.21}Ga_{0.79}As$ pHEMTs with a 15.5 nm and 15.0 nm channel width grown on LTDD and HTDD GaAs substrates, respectively.
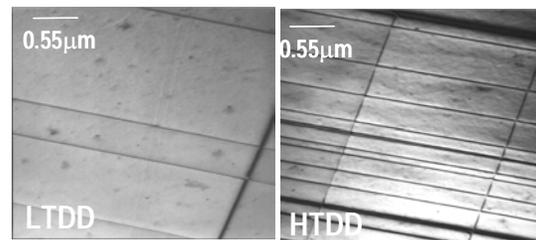

Figure 4. Plan-view TEM image of $In_{0.21}Ga_{0.79}As$ pHEMTs with a 22 nm and 21 nm channel width grown on LTDD and HTDD GaAs substrates, respectively.

A similar behavior is illustrated in figure 5 where the channel Hall conductivity is plotted as a function of channel layer thickness. The Hall conductivity is measured on pHEMT structures without doped caps (50 nm n$^+$ GaAs) but, in all other aspects, identical to the device structure shown in figure 1. The decrease in the Hall conductivity with increasing channel layer thickness is due to the presence of misfit dislocations and possibly threading dislocations. The decrease is significantly greater for the HTDD samples.

Figure 6 illustrates the impact of the LTDD and HTDD substrates on the peak transconductance (G_{MP}) and cut-off frequency (F_T). As the channel thickness increases from 14 to 16 nm, G_M and F_T increase for both substrate types. From 15 to 16 nm the devices grown on LTDD substrates continue to show increasing performance while devices grown on HTDD substrates show decreasing performance.
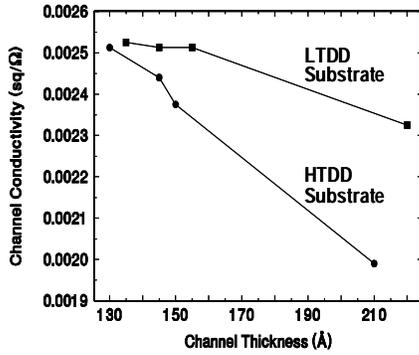
Figure 5. Hall conductivity as a function of channel thickness showing a greater decrease for the HTDD substrates.
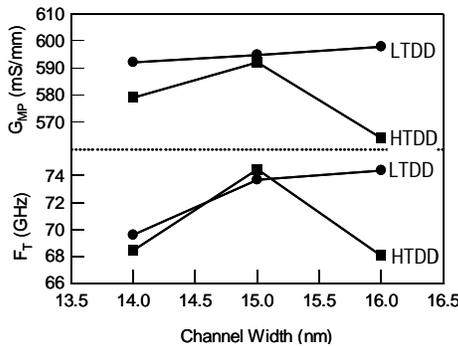

Figure 6. pHEMT peak transconductance and cut-off frequency showing increased performance at thicker channels for devices grown on LTDD material.

AlGaN/GaN HEMT

The high breakdown fields, high electron saturation velocity, and high electron densities in AlGaN/GaN HEMT structures have led to demonstrated microwave power performance that significantly exceeds that of state-of-the-art GaAs and InP-based devices [7-8]. Low-noise, high breakdown GaN HEMTs [8-10] in amplifier front-ends eliminate the need for diode limiters as protection against RF overstress. This can reduce the overall LNA noise figure by 1 dB. High linearity GaN HEMT power amplifiers with high power added efficiencies [11] have the potential to replace traveling-wave tube amplifiers. These solid-state GaN amplifiers would offer lower weight, higher reliability, and lower cost. This has resulted in a significant development effort of this material system.

Because of a lack of a native GaN substrate, AlGaN/GaN HEMT epitaxial layers are nominally grown on sapphire or semi-insulating (SI) SiC substrates. For device wafers, we grow on SiC substrates because of our ability to fabricate through vias and thin the substrates using our nominal III-V fabrication capability. In addition, SiC offers high thermal conductivity than sapphire substrates, 3.4 W/cm-K and 0.42 W/cm-K, respectively. We use sapphire substrates for calibration purpose. The maturity of SI SiC substrates is not equal to that of the GaAs and InP substrates. Therefore, it is critical to understand the impact of the substrate imperfections on the epitaxial layers and on device performance. We report on some initial correlation activities to identify the impact of the 4-H SI SiC substrate structures on the epitaxial layers.

Polishing scratches are a significant issue with SiC substrates as-received from the substrate vendors. Figure 7 illustrates the surface condition of as-received SI SiC substrates. A significant density of gross scratches is visible in optical images. Atomic force microscopy (AFM) imaging reveals a higher density of micro-scratches. Figure 8 shows that the scratches are clearly visible in the epitaxial films after MBE growth. Figure 8 also shows the very smooth MBE topology possible on SiC substrates after a chemical-mechanical polish (CMP) performed by an outside vendor.
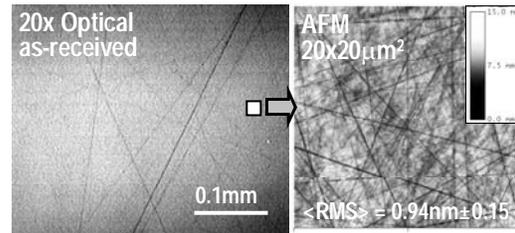

Figure 7. Typical as-received SI SiC surface. Several large scratches are seen in the optical image. The AFM image reveals a high density of micro-scratches.
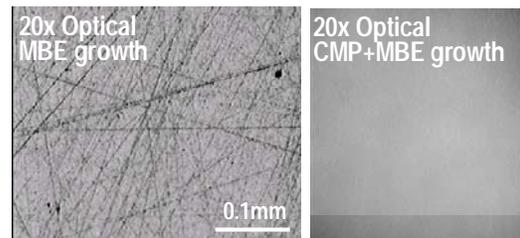

Figure 8. Optical image of an AlGaN/GaN HEMT epitaxy layer grown on an as-received SI SiC substrate (left) and after a chemical-mechanical polish (right).

Micropipe densities in SI SiC substrates are not specified by the vendors due to an inability to decorate them with a chemical etch. Micropipe decoration facilitates automatic counting of the defects. Therefore, it is very difficult to determine the impact of substrate micropipe density on device performance on a wafer scale. However, micropipes are not distributed uniformly across the substrate but tend to cluster. This enables us to investigate these localized regions. Figure 9 shows the impact of micropipes on metal-organic chemical vapor deposition (MOCVD) grown epitaxial layers. Under certain growth conditions, the micropipes act as nucleation sites for the formation of 0.2 - 0.3 µm tall circular mounds to form in the epitaxial layer. These mounds impact the ability to process these wafers by interfering with stepper registry or by causing photoresist lift-off during contact lithography. In addition, the micropipe cluster region shows several grain boundaries. For MBE grown material, we have not found the mound formation but we do see the grain boundaries in the micropipe clusters.
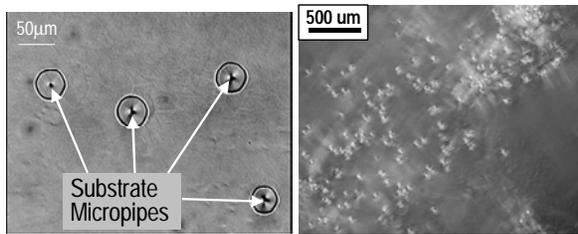
Figure 9. Optical image of circular epitaxial features (left) nucleated at micropipes in the SiC substrate. These features are 0.2 - 0.3 μm tall and 40-50 μm in diameter. These epitaxial features are localized due to clustering of micropipes (right) with densities around 1.9×10^3 cm^{-2}.

We employed double crystal reflection x-ray topography to image dislocations, micropipes, and low angle boundaries in the SiC substrates and the epitaxial GaN layers of processed AlGaN/GaN HEMT wafers grown by MBE and MOCVD. X-ray topograph images were taken before epitaxial growth, after epitaxial growth, and after processing. The defects in the substrates were not measurably changed after the epitaxial layer deposition, but the wafers did exhibit more curvature, as would be expected from the stress introduced by the slightly mismatched nitride layers. Even though the GaN layer peak possessed a much greater full width at half maximum ($\approx$ 200 arcsec) than the SiC substrate peak ($\approx$ 20 arcsec), the micropipes and tilt boundaries from the SiC substrate produced structural defects in the GaN layers as did other defects such as inclusions. Figure 10 shows the x-ray topographs of the $(11\bar{2}4)$ GaN reflection and the $(11\bar{2}8)$ SiC reflection. Several structures in the GaN epitaxial layer with corresponding structures in the SiC substrate have been highlighted. A clear one-to-one correlation between SiC substrate defects and GaN defects exists. There was also evidence that – in a few cases – crystallographic defects in the epitaxial film did not originate with substrate defects. We are currently in the process of identifying the true nature of the structures and determining their impact on the device performance.
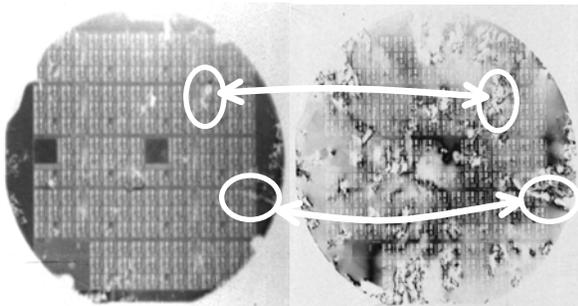

Figure 10. X-ray topograph of the $(11\bar{2}4)$ GaN reflection (left) and the $(11\bar{2}8)$ SiC reflection (right) from a fabricated HEMT wafer. The arrows and circles highlight several features from the substrate that appear in the epitaxial layer.

Summary

Substrate quality is critical for device performance and yield. For GaAs based pHEMT devices the threading dislocations in the substrate act as nucleation sites for misfit dislocation formation in the strained channel layer. Using LTDD GaAs substrates allows thicker or higher indium content pHEMT channels than HTDD substrates which enables improved device performance. The presence of epitaxial defects does not necessarily impact the performance. For the GaAs pHEMTs, the device performance is improved up to the point that an orthogonal array of defects is formed.

For the AlGaN/GaN material system, we have shown that substrate scratches, micropipes, and crystal structures identified by x-ray topography impact the epitaxial layer quality. Scratches are eliminated through the use of external vendor CMP. Micropipes tend to cluster with densities as high as 1.9×10^3 cm^{-2} so their impact is limited to the clustered region. X-ray topography clearly shows that substrate features are reproduced in MBE and MOCVD grown epitaxial material. The nature of these structures and their impact on device performance is not clear and requires further investigation.

References

[1] H. Wang, L. Samoska, T. Gaier, A. Peralta, H.-H. Liao, Y. C. Leong, S. Weinreb, Y. C. Chen, M. Nishimoto, and R. Lai, *IEEE Trans. Microwave Theory Tech.* **49**, 9 (2001).

[2] E. Y. Chang, D.-H. Lee, S. I. Chen, and H. C. Chang, *Electronics Lett.* **36**, 577 (2000).

[3] M. Meshkinpour, M. S. Goorsky, B. Jenichen, D. C. Streit, and T. R. Block, *J. Appl. Phys.* **81**, 3124 (1997).

[4] A. Iida and K. Kohra, *Phys. Status Solidi A* **51**, 533 (1979).

[5] R. Sandhu, G. Bhasin, C. D. Moore, G. D. U'Ren, M. S. Goorksy, T. P. Chin, M. Wojtowicz, T. R. Block, and D. C. Streit, *J. Vac. Sci. Technol. B* **17**, 1163 (1999).

[6] M. Meshkinpour, M. S. Goorsky, G. Chu, D. C. Streit, T. R. Block, and M. Wojtowicz, *Appl. Phys. Lett.* **66**, 748 (1995).

[7] L.F. Eastman, *Cornell University's 20th Final Quarterly Report under MURI Contract No. N0014-96-1-1223*.

[8] I.P. Smorchkova, M. Wojtowicz, R. Sandhu, R. Tsai, M. Barsky, C. Namba, P.-S. Liu, R. Dia, M. Truong, D. Ko, J. Wang, H. Wang, and A. Khan, *Proc. of 2002 IEEE Les Eastman Conf. on High Performance Devices*, 422 (2002).

[9] W. Lu, J. Yang, M.A. Khan, and I. Adesida, *IEEE Trans.Electron.Dev.* **48**, 581 (2001).

[10] J.S. Moon, M. Micovic, P. Janke, P. Hashimoto, W.S. Wong, R.D. Widman, L. McCray, A. Kurdoghlian, and C. Nguyen, *Electronics Lett.* **37**, 528 (2001).

[11] R. Sandhu, M. Wojtowicz, I. Smorchkova, M. Barsky, R. Tsai, J. W. Yang, H. Wang, M. A. Khan, *Proc. of 60th Device Research Conf.*, 27 (2002).